scientific reports

Check for updates

OPEN

Comprehensive model for simultaneous monitoring of primary tumor to metastatic cancer utilizing *Prkdc* and *Il2rg* double knockout mice

Hee Jung Kwon[1,2], Jang Woo Park[3], Hye Kyung Chung[3] & Joohee Jung[1,2]✉

Liver cancer is the second leading cause of cancer-related deaths worldwide, motivating major scientific efforts to understand and treat this cancer type. Over 30% of patients with liver cancer progress to metastasis, which reduces the survival rate. Extensive studies on primary tumors have been conducted to improve the prognosis. However, there is a lack of appropriate and accessible models for studying the progression and metastasis of liver cancer. Moreover, conventional metastasis models do not reproduce metastasis as it occurs in patients. To address this lack of an appropriate model for the monitoring of cancer progression and evaluation of anticancer drugs, we established a spontaneous metastatic xenograft model using NSG mice subcutaneously transplanted with SK-Hep-1 cells. Compared to the conventional experimental metastasis model (intravenous transplantation), in which only lung metastasis was observed, the established spontaneous metastatic xenograft model was superior, as it showed both a primary tumor and metastatic patterns similar to those observed in human patients. Additionally, this model was successfully used to assess the antimetastatic efficacy of sorafenib. In conclusion, our results demonstrate that the established spontaneous metastatic xenograft model better reflects liver cancer metastasis and can be utilized to assess the efficacy of anticancer drugs for liver cancer.

Keywords Liver neoplasms, Mice, Neoplastic processes, Sorafenib, Survival rate, Xenografts

Cancer was the second leading cause of death in 2019[1], although its mortality rate has shown a declining trend, which can be attributed to extensive research efforts[2]. Nevertheless, cancer recurrence and metastasis remain limiting factors associated with a low survival rate[3]. Therefore, research on cancer progression and the development of novel anticancer strategies are needed.

Diverse experimental models have been established to simulate cancer progression. The complicated interactions between cancer cells and other cells, such as immune cells, stroma cells, and vascular endothelial cells, are reflected in in vivo models rather than in vitro models[4]. A human-derived xenograft model is a useful system to investigate liver cancer in the context of human cancer biology, particularly focusing on the tumor microenvironment and therapeutic responses. Therefore, we used SK-Hep-1 cells to establish the human-derived xenograft model in this study. SK-Hep-1 cells, a human hepatic adenocarcinoma cell line that originated from human liver sinusoidal endothelial cells[5], are commonly used for liver cancer research because the cells are known to form hepatocarcinoma tumors[6]. To establish a xenograft mouse model, cancer cells of human origin are transplanted into immune-deficient mice lacking T cells, B cells, and natural killer (NK) cells, which play key roles in immune responses[7]. Genetic modifications targeting key genes, such as Forkhead box N1, recombination activating gene 2 (*Rag2*), and catalytic polypeptide of DNA-dependent protein kinase (*Prkdc*), enable the generation of T cell- and B cell-deficient strains, such as athymic nude, *Rag2*, and severe combined immunodeficiency (SCID) mice[8]. Additionally, mice with compromised NK cell function, attributed to gene losses in *IL2rg* and *B2m*, contribute to the range of available models. Through strategic breeding, NOD-SCID mice or more profoundly immunodeficient NSG (NOD-SCID *IL2rg* null) mice can be produced[9]. These mouse

[1]College of Pharmacy, Duksung Women's University, Seoul 01369, Korea. [2]Duksung Innovative Drug Center, Duksung Women's University, Seoul 01369, Korea. [3]Korea Radioisotope Center for Pharmaceuticals, Korea Institute of Radiological and Medical Sciences, Seoul 01812, Korea. ✉email: joohee@duksung.ac.kr

models exhibit compromised overall immune defenses owing to the absence of T, B, and NK cells, rendering them particularly susceptible to tumor growth and transplantation studies[10]. The selection of specific mouse strains is tailored to the unique objectives of each research study, emphasizing their crucial role as invaluable models for investigating diverse facets of diseases.

Xenograft mouse models are used to assess the efficacy of anticancer drugs in the preclinical stage, and are classified based on the sites where cancer cells are transplanted[11]. Ectopic xenograft models involve the subcutaneous transplantation of cancer cells into the back or legs of mice. This model type is broadly used because of its user-friendliness, high tumorigenicity, and easy observation of tumor growth. However, it does not replicate the original cancer environment; therefore, cancer metastasis does not occur. In orthotopic xenograft models, cancer cells are transplanted into the organ from which the cancer originated. Hence, this model can mimic the microenvironment of the primary cancer, but has several disadvantages, such as requiring highly skilled techniques in researchers and advanced monitoring equipment. Moreover, metastasis occurrence is rare. To investigate metastasis, transplantation through the tail vein of mice is often performed. However, this experimental metastasis model bypasses the invasion of cells from the primary cancer site, and metastasis primarily occurs in the lung or liver, which may not reflect metastatic sites in patients. Unfortunately, a xenograft model to monitor the natural progression of liver cancer from the primary cancer to metastatic lesion has not yet been established. To address this gap, in the present study, a spontaneous metastatic xenograft model was established using NSG mice to monitor liver cancer progression and assess the efficacy of anticancer drugs.

Results

Establishment of a spontaneous metastatic xenograft model using NSG mice

We established a spontaneous metastatic xenograft model by injecting the liver cancer SK-Hep-1 and SK-Hep-1_Luc cell lines into NSG mice. After subcutaneous injection of SK-Hep-1 cells, tumor sizes were measured twice per week for 40 days. Two weeks post-injection of the cells, SK-Hep-1-derived tumors could be observed with the naked eye. From three weeks post-injection, the tumor volume significantly increased. Between 14 and 40 days, the increase in tumor volume was nearly 6-fold, from 120 mm^3 to 720 mm^3 (Fig. 1a).

The uptake of [18 F]-2-fluoro-2-deoxy-D-glucose (18 F-FDG) in the SK-Hep-1 cell-derived xenograft models was confirmed using positron emission tomography (PET) and computed tomography (CT) imaging (Fig. 1b). On PET-CT images, the tumors appeared as yellow and pink areas. The transplanted site (Fig. 1b; white arrows) was markedly observed, and metastatic lesions (Fig. 1b; yellow arrows) were observed in the liver, intestine, and lymph nodes. In the model implanted with SK-Hep-1_Luc cells, tumors were monitored in real time using luciferase activity (Fig. 1c). Metastasis was detected in one mouse (in the armpit) at 4 weeks and in all mice at 5 weeks after injection of SK-Hep-1_Luc cells. Through bioimaging techniques, we could confirm metastatic cancer as the findings demonstrated that the subcutaneously implanted cancer cells invaded and spontaneously metastasized to multiple organs in the mice.

Differences between the subcutaneously established spontaneous metastatic xenograft and conventional experimental metastasis models

The main difference between the established spontaneous metastatic xenograft model and the conventional experimental metastasis model was the transplantation site. Metastatic lesions were investigated between the two models depending on the site of cancer cell transplantation. In the conventional experimental metastasis model, cells were injected via the tail veins, whereas in the established spontaneous metastatic xenograft model, cells were implanted subcutaneously, and metastasis occurred spontaneously. In both models, mice were sacrificed 8 weeks post-transplantation and dissected. In both models, liver metastasis was highly successful; however, there were differences between the two methods with respect to metastasis in other organs. In the conventional experimental metastasis model, liver and lung metastasis was observed (black arrow, Fig. 2a), and metastasis was not observed in any other organs (Fig. 2a). On the other hand, metastasis was observed in the lung, kidney, colon, bone, and lymph node (armpit) in the established spontaneous metastatic xenograft model (black arrow, Fig. 2b). A significant increase in lymph node metastases was observed in the spontaneous metastasis model when the number of mice with metastases to multiple organs was compared between the two transplantation methods (Fig. 2c). Metastasis to the kidney occurred significantly only in the spontaneous metastasis model. The area of metastatic lesions relative to the total liver tissue was similar between the conventional experimental metastasis model and spontaneous metastatic xenograft model (Fig. 2d and e). However, metastatic lesions of the liver, lymph nodes, and kidneys occurred in the spontaneous metastatic xenograft model and were observed by H&E staining and Ki-67 expression level (Fig. 2f), indicating active proliferation, particularly within the metastatic lesions.

Efficacy assessment of anticancer drug for liver cancer progression in spontaneous metastatic xenograft model

An advantage of the established spontaneous metastatic xenograft model is that it can help evaluate the growth of both primary cancer and metastasis in the same mice. To investigate the use of this model for the evaluation of metastatic agents, sorafenib was orally administrated.

Tumor growth was compared between control and sorafenib-treated mice using a caliper (Fig. 3a). Primary tumor growth did not differ between the two groups. As shown in Fig. 3b, the luminescence intensity of the transplanted site increased with time, indicating that the primary tumor was growing (dorsal side) consistent with Fig. 3a. However, the luminescent metastatic sites were significantly different between the control and sorafenib-treated mice (ventral side): while luminescence intensity in metastatic lesions was detected within one week in control mice, it was only observed after four weeks in sorafenib-treated mice (Fig. 3b). Further,

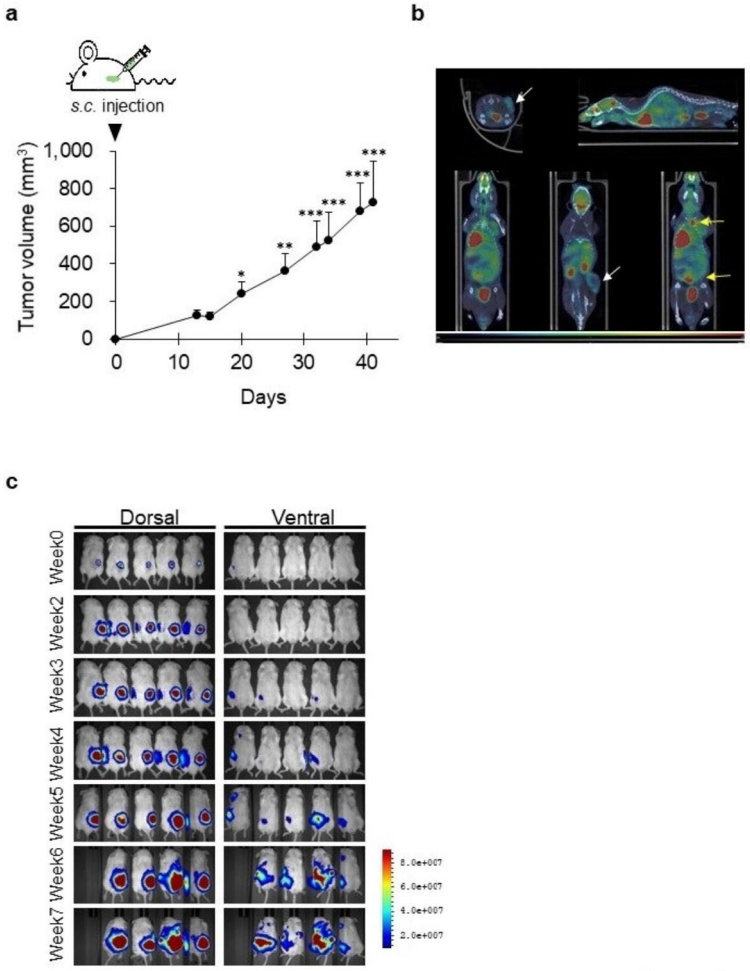

Fig. 1. Establishment of a spontaneous metastasis model in NSG mice. (**a**) Tumor growth curve of the SK-Hep-1 cell-derived xenograft model. Data are presented as the mean ± standard deviation ($n = 6$). *, $p < 0.05$, **, $p < 0.001$, *** $p < 0.0001$ (one-way ANOVA, Dunnett's post hoc test). *s.c.*, subcutaneous. (**b**) Positron emission tomography (PET) and computed tomography (CT) images of spontaneous metastasis models. White arrow, transplanted site. Yellow arrow, metastatic lesion. (**c**) Bioluminescence images of spontaneous metastasis models. SK-Hep-1_Luc cells were subcutaneously injected into NSG mice ($n = 5$). Tumor growth and metastasis were observed once a week for 5 weeks.

luminescence intensity was significantly lower in the sorafenib-treated group compared to that in the control group (Fig. 3b). After the final imaging, the luminescence of the isolated tissues was detected. Metastasized tumor tissues in the liver and kidneys showed luminescence in the control but not in the sorafenib-treated mice (Fig. 3c). Several tumors were observed with the naked eye, despite limited detection by the in vivo imaging system (Fig. 3c). These findings indicate that the established spontaneous metastatic xenograft model can be used to evaluate the anti-metastatic efficacy of sorafenib and other anti-metastatic agents.

Discussion

Cancer research continues to progress with substantial advancements; however, the complexity of cancer poses a significant challenge. Current cancer research not only focuses on suppressing proliferation and inducing apoptosis, but also on metastasis inhibition by studying how tumors spread to different organs. Metastasis inhibition research has gained prominence as an important domain in cancer research, as metastasis increases the difficulty of treatment and lowers patient survival rates. Consequently, animal experiments are indispensable in translational cancer research, given the limitations of in vitro experiments. Through animal studies, we have gained valuable insights into the mechanisms of cancer metastasis, which have contributed to the development of effective therapeutic strategies.

Immunodeficient mice, exhibiting varying levels of immunodeficiency based on the mouse strain, are commonly employed in cancer research. In particular, NSG mice, which are derived from the crossbreeding of NOD/SCID mice with mice carrying *IL2 rg* null, resulting in the absence of T cells and B cells, loss of C5 complement, reduced NK cell activity, and inactivation of the innate immune system, are commonly used. Given that NSG mice have more pronounced immune deficiency compared to NOD/SCID mice, they exhibit higher

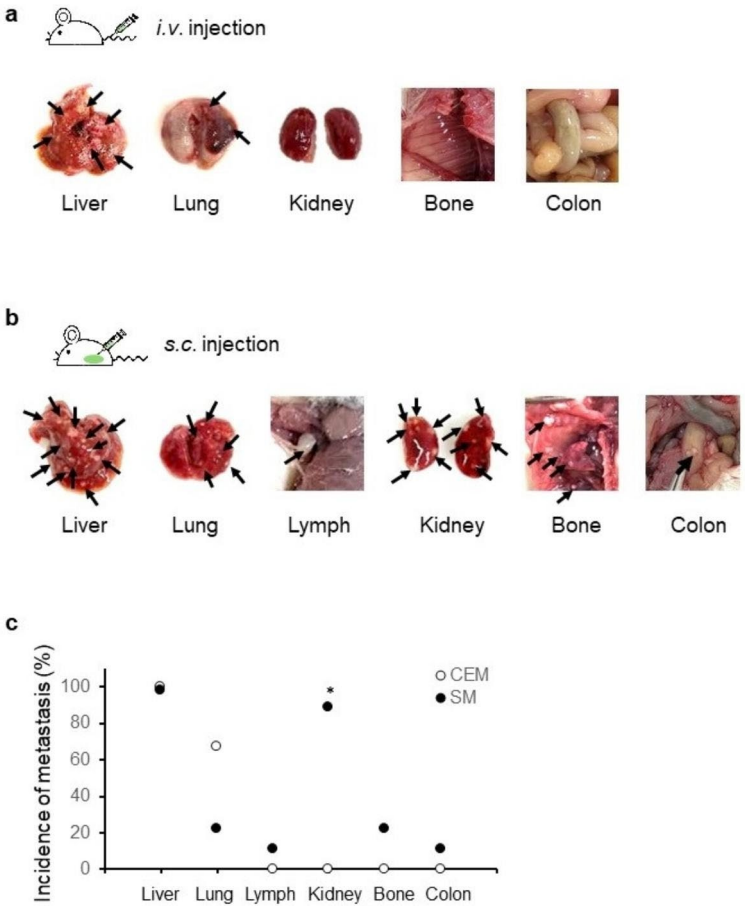

Fig. 2. Comparison of metastatic lesions between intravenous (*i.v.*) and subcutaneous (*s.c.*) transplantation. (**a**) Metastatic lesions in the conventional experimental metastasis model. SK-Hep-1 cells were intravenously transplanted into NSG mice ($n=5$). (**b**) Metastatic lesions in the spontaneous metastatic xenograft model. SK-Hep-1 cells were subcutaneously implanted into NSG mice ($n=5$). Black arrow, metastatic lesion. (**c**) Comparison of metastatic lesions between two metastatic models in NSG mice. Data are expressed as the proportion of mice with metastases to multiple organs compared with the entire experimental group (Fisher's exact test). *, $p<0.05$. CEM, Conventional experimental metastasis model; SM, spontaneous metastasis model. (**d**) Hematoxylin-stained liver tissues. The red dashed lines indicate the metastatic lesions. CEM, Conventional experimental metastasis model; SM, spontaneous metastasis model. Scale bar, 500 μm. (**e**) Quantification of metastatic lesion in liver tissues. Data are expressed as the mean ± standard deviation ($n=3$ / group). (**f**) Expression of Ki67 in metastatic lesions of organs (liver, lymph nodes, kidneys) in the spontaneous metastasis model. Scale bar, 100 μm.

tumor engraftment with occurrence of metastasis due to the complete knockout of receptors capable of binding to cytokines, surpassing NOG mice in this aspect[11].

When transplanting breast cancer cells[10] and neuroblastoma cells[12] into NSG mice, metastases were observed more frequently in various organs compared to those in transplanted nude mice. Our data using MDA-MB-231 breast cancer cells are similarly consistent with previous reports (Supplementary data 1). In the present study, to the best of our knowledge, we are the first to report that liver cancer progression could be simulated by establishing a spontaneous metastatic xenograft model. In this model, we used SK-Hep-1 cells instead of human hepatocellular carcinoma cell lines, such as HepG2 and Huh7 cells. HepG2 and Huh7 cells have been reported to not form solid tumors as reliably in xenograft models[13,14]. Therefore, in HepG2 or Huh7-derived tumors, it is difficult to observe histologic properties and obtain clear luminescence images because of interference from blood-related luminescence. As a result, SK-Hep-1 cells provided a more suitable model for the visualization and histological analysis in the assessment of tumor progression. Utilizing NSG mice in xenograft experiments with a human liver cancer cell line, we confirmed effective tumor engraftment, growth, and subsequent metastasis (Fig. 1). In human patients with liver cancer, there are common sites of metastasis, with occurrences predominantly in the lungs, portal vein, portal lymph nodes, intra-abdominal lymph nodes, and bones[15]. Interestingly, when transplanting liver cancer cell lines into NSG mice, the observed locations of tumor metastasis closely resembled those in human patients with liver cancer (Fig. 2b). Consistent with our results, human melanoma metastasis in NSG mice also correlated with that observed in human patients[16].

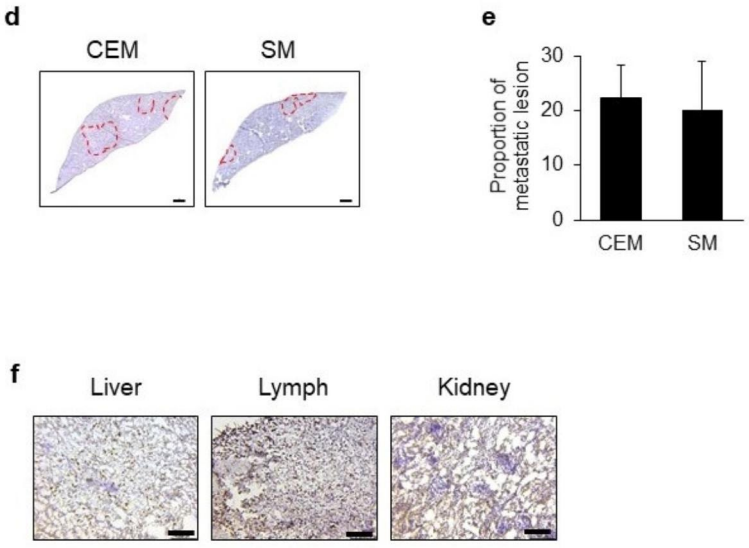

Figure 2. (continued)

In summary, we developed a spontaneous metastatic xenograft model for the assessment of cancer progression and efficacy of anticancer drugs. Our approach involves subcutaneous injection of liver cancer cells in NSG mice for the spontaneous generation of a metastatic cancer model, resulting in a model that exhibits characteristics similar to those of human liver metastatic cancer. Compared with the conventional metastasis model, the spontaneous metastatic cancer model exhibited similar metastatic lesions in the liver; however, the spontaneous model allowed for the analysis of metastatic lesions across a broader range of organs, including the kidneys, lymph nodes, and bones. Our experimental animal model mimics spontaneous metastasis, overcoming the absence of primary tumors in other conventional experimental metastatic models. Nonetheless, histopathological studies and further validation are needed to establish the proposed model as a promising model for research on cancer progression and metastasis. Additionally, it is important to highlight that our method is considerably more straightforward compared to models created through orthotopic transplantation. As orthotopic transplantation involves the transplantation of cancer cells into primary organs to induce spontaneous metastasis, it requires advanced surgical procedures, especially in organs such as the liver and colon, making the experimenter's skill a crucial factor for the successful establishment of a model. By facilitating accessibility for researchers, our approach significantly reduces barriers to the development of metastatic cancer models and would hence facilitate research on cancer progression and metastasis.

Methods

Ethical statement

The animal study protocol was approved by the Duksung Women's University Institutional Animal Care and Use Committee (2022-001-013).

Cell culture

The SK-Hep-1 human liver cancer cell line was purchased from the Korean Cell Line Bank and was maintained in Dulbecco's modified Eagle's medium (GenDEPOT, Katy, TX, USA). SK-Hep-1_Luc cells (luciferase-expressing cells) were kindly provided by Prof. S. Kuroda (Osaka University, Japan) and maintained in Eagle's Minimum Essential Medium (GenDEPOT). Both cell types were cultured in a 5% carbon dioxide incubator at 37 °C in media supplemented with 10% fetal bovine serum (GW Vitek, Seoul, South Korea) and 1% penicillin–streptomycin (GenDEPOT).

Animals

All animal experiments were performed in compliance with the guidelines for the care and use of laboratory animals of the Duksung Women's University Institutional Animal Care and Use Committee. Male NOD/Prkdc^{em1Baek} Il2rg^{em1Baek} (NSG) mice (5-weeks-old) were purchased from JA BIO (Suwon, South Korea). The mice were allowed to acclimatize for one week before the start of experiments. The laboratory conditions were maintained at a temperature of 20 °C, with a 50% humidity level, and a 12-hour light/12-hour dark cycle was followed. The mice were provided with drinking water *ad libitum*.

Procedure for transplantation of liver cancer cells in xenograft models

After acclimatization for one week, SK-Hep-1_Luc cells (1×10^6 cells/100 μL of PBS) were intravenously injected into the tail vein of NSG mice as slowly as possible for the conventional experimental metastatic model. For the spontaneous metastasis model, SK-Hep-1 or SK-Hep-1_Luc cells (5×10^6 cells/100 μL of PBS) were subcutaneously implanted into the right flank of NSG mice.

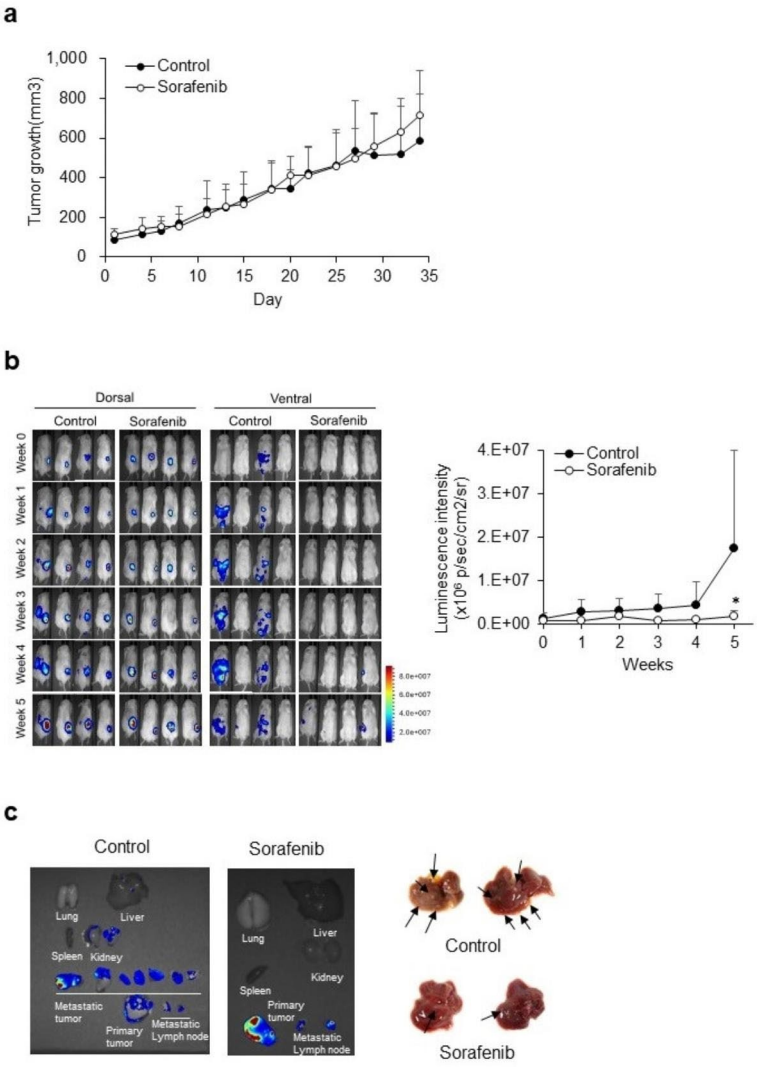

Fig. 3. Monitoring of tumor growth and metastasis in the spontaneous metastatic xenograft model. (**a**) Tumor growth in the control and sorafenib-treated groups. Data are presented as the mean ± SD ($n = 4$/group). (**b**) Comparison of luminescence between the control and sorafenib-treated groups. Dorsal images show the growth of primary tumor with time. Ventral images show metastatic lesions. Quantification of luminescence intensity. Data are presented as the mean ± SD ($n = 4$/group). *, $p < 0.05$ (two-way analysis of variance with Sidak's post hoc test). (**c**) Isolated tumor tissues.

Measurement of tumor growth

Tumor size was measured twice per week. Tumor volume was calculated using the following equation:

$$\text{Tumor volume } (mm^3) = (\text{longest length} \times [\text{shortest length}]^2)/2.$$

PET and CT imaging

PET-CT imaging was performed on a small animal NanoScan (Mediso Medical ImagingSystems, Budapest, Hungary). Mice were anesthetized with isoflurane and injected with 7.4 MBq of 18 F-FDG in 200 µL of saline (PBS) through the tail vein. PET images were obtained with an energy window of 400–600 keV for 20 min, one hour after tracer administration. For attenuation correction and anatomical reference, micro-CT imaging was performed 2 min before PET imaging at 50 kVp of X-ray voltage and 580 µA of anode current (exposure per projection 170 ms, 1:4 binning). Static PET images were reconstructed using a three-dimensional ordered subset expectation maximization (3D-OSEM) algorithm with four iterations, six subsets, and an isotropic 0.4-mm voxel dimension.

In vivo imaging

The established spontaneous metastasis model was subjected to bioluminescence imaging to monitor the primary tumor growth and metastasis. Bioluminescence imaging of luciferase activity was performed using an in vivo system (Visque® InVivo Elite, Vieworks, Gyeonggi, South Korea). Mice anesthetized with 2% isoflurane (Piramal Pharma Solutions, Mumbai, India) were intraperitoneally injected with D-luciferin (150 mg/kg, PerkinElmer,

Waltham, MA, USA). After anesthesia, photos were taken with an exposure time of 10 min each on the dorsal and ventral sides. Imaging was repeated once a week.

Sorafenib treatment

NSG mice were transplanted with SK-Hep-1_Luc cells as described in the section *Procedure for transplantation of liver cancer cells in xenograft models* and randomly divided into two groups (control and sorafenib-treated). Sorafenib (10 mg/kg bw/10 mL) was orally administered daily from the day of transplantation until the end of the experimental period (5 days/weeks).

Immunohistochemistry and hematoxylin staining

Tumor tissues isolated from SK-Hep-1-cell-derived xenografts were embedded in an optimal cutting temperature compound and snap-frozen in isopropanol using liquid nitrogen. Tissue Sect. (5 μm) were obtained using a cryostat (Leica, Nussloch, Germany). Each slide section was rehydrated with tap water and incubated with 3% H_2O_2 in methanol to quench endogenous peroxidase activity. The sections were stained with anti-Ki67 antibody (1:200; Abcam, MA, USA) overnight at 4 °C. Antigen-antibody reactions were visualized using the EnVision + Dual Link System-HRP (Vector Laboratories, CA, USA) and 3,3′-diaminobenzidine (Vector Laboratories). The stained sections were dehydrated, counterstained with hematoxylin (Sigma-Aldrich) and mounted in limonene mounting medium (Abcam). The slides were observed under a light microscope (Leica Microsystems Ltd., Wetzlar, Germany).

Statistical analysis

Data were represented as the mean ± standard deviation (SD). Statistical significance was assessed using analysis of variance and Fisher's exact test using GraphPad Prism 7 (GraphPad Software Inc., San Diego, CA, USA). Statistical significance was set at $p < 0.05$.

Data availability

All data are available in this manuscript and supplementary data.

Received: 18 July 2024; Accepted: 7 October 2024
Published online: 09 October 2024

References

1. Xu, J., Murphy, S. L., Kochanek, K. D. & Arias, E. Deaths: final data for 2019. *NCHS Natl. Vital Stat. Rep.* **70** https://doi.org/10.15620/cdc:106058 (2021).
2. Kang, M. et al. Cancer statistics in Korea: incidence, mortality, survival, and prevalence in 2020. *Cancer Res. Treat.* **55**, 385–399 (2023).
3. Siegel, R. L., Miller, K. D., Fuchs, H. E. & Jemal, A. Cancer statistics, 2022. *CA Cancer J. Clin.* **72**, 7–33 (2022).
4. Porter, R. J., Murray, G. I. & McLean, M. H. Current concepts in tumour-derived organoids. *Br. J. Cancer*. **123**, 1209–1218 (2020).
5. Tai, Y. et al. SK-Hep1: not hepatocellular carcinoma cells but a cell model for liver sinusoidal endothelial cells. *Int. J. Clin. Exp. Pathol.* **11**, 2931–2938 (2018).
6. Puttahanumantharayappa, L. D., Gowda, S., Shiragannavar, N. G., Santhekadur, P. K. & V. D. & Origin and properties of hepatocellular carcinoma cell lines. *Jpn J. Gastroenterol. Res.* **1**, 1–5 (2021).
7. Jung, J. Human tumor xenograft models for preclinical assessment of anticancer drug development. *Toxicol. Res.* **30**, 1–5 (2014).
8. Belizário, J. E. Immunodeficient mouse models: an overview. *Open. Immunol. J.* **2**, 79–85 (2009).
9. Ito, R., Takahashi, T., Katano, I. & Ito, M. Current advances in humanized mouse models. *Cell. Mol. Immunol.* **9**, 208–214 (2012).
10. Puchalapalli, M. et al. NSG mice provide a better spontaneous model of breast cancer metastasis than athymic (nude) mice. *PLOS One*. **11**, e0163521 (2016).
11. Neff, E. Models matter in metastasis. *Lab. Anim.* **46**, 3 (2017).
12. Sartelet, H., Durrieu, L., Fontaine, F., Nyalendo, C. & Haddad, E. Description of a new xenograft model of metastatic neuroblastoma using NOD/SCID/*Il2rg* null(NSG) mice. *Vivo*. **26**, 19–30 (2012).
13. Knowles, B. B., Howe, C. C. & Aden, D. P. Human hepatocellular carcinoma cell lines decrete the major plasma proteins and hepatitis B surface antigen. *Science*. **209**, 497–499 (1980).
14. Song, Y., Lu, Q., Jiang, D. & Lan, X. Validation and utility of HepG2 xenograft model for hepatocellular carcinoma. *Eur. J. Nucl. Med. Mol. Imaging*. **50**, 639–641 (2023).
15. Protopapa, M. N., Lagadinou, M., Papagiannis, T., Gogos, C. A. & Solomou, E. E. Hepatocellular carcinoma: An uncommon metastasis in the orbit. *Case Rep. Oncol. Med.* 7526042 (2020). (2020).
16. Quintana, E. et al. Human melanoma metastasis in NSG mice correlates with clinical outcome in patients. *Sci. Transl Med.* **4**, 159ra149 (2012).

Acknowledgements

We would like to thank Editage (www.editage.co.kr) for English language editing.

Author contributions

Conceptualization, J.J.; methodology, H.J.K., J.W.P., H.K.C.; validation, J.J., H.J.K.; formal analysis, H.J.K.; investigation, H.J.K.; data curation, H.J.K., J.W.P., H.K.C.; writing-original draft preparation, H.J.K.; writing-review and editing, J.J.; visualization, H.J.K., J.J.; supervision, J.J.; project administration, J.J.; funding acquisition, J.J. All authors have read and agreed to the published version of the manuscript.

Funding

This research was funded by an NRF grant by the MSIT (NRF-2021R1A2C2004535), the Priority Research Centers Program through an NRF funded by the Ministry of Education (2016R1A6A1A03007648).

Declarations

Competing interests
The authors declare no competing interests.

Additional information
Supplementary Information The online version contains supplementary material available at https://doi.org/10.1038/s41598-024-75493-z.

Correspondence and requests for materials should be addressed to J.J.

Reprints and permissions information is available at www.nature.com/reprints.

Publisher's note Springer Nature remains neutral with regard to jurisdictional claims in published maps and institutional affiliations.